Supporting Information for: How β-Phase Content Moderates Chain Conjugation and Energy Transfer in Polyfluorene Films

Hannah J. Eggimann, Florian Le Roux, Laura M. Herz*

Department of Physics, University of Oxford, Clarendon Laboratory, Parks Road, Oxford, OX1 3PU, United Kingdom

E-mail: laura.herz@physics.ox.ac.uk

Contents

1 Sample Preparation

We prepared a series of thin films of poly(9,9-dioctylfluorene) (PFO) with varying content of β-phase chain segments. The PFO thin film samples (PFO received from Cambridge Display Technology[1] with peak molecular weight, $M_p = 133\,000\,\mathrm{g\,mol^{-1}}$) were deposited on pre-cleaned quartz substrates by spin-coating (2000 rpm for one minute). Both, solutions and substrates, were pre-heated at 80 °C for 5 minutes immediately prior to deposition. Following deposition, the substrates were annealed for 1 minute at 120 °C to remove any traces of solvent. The β-phase chain segment fractions were tuned from 0% (all glassy phase) to 25.6% (as demonstrated in Ref.[2]) by adding 100 µL aliquots of increasing concentration (0 µL to 80 µL per mL) of paraffin oil (Edwards[3] Ultragrade 19) in toluene solutions to 1.9 mL portions of a baseline 13.5 mg per 1 mL PFO in toluene solution. This procedure yields mixtures with 0 to 0.4 vol% paraffin oil. Samples were prepared with different β-phase fractions (see Table 1), which we determined from the relative strength of the duly weighted (to correct for the known oscillator strength increase), integrated absorption contribution (see Section 2).

We measured the thickness of each film using a Dektak profilometer (Table 1). The percentage of β-phase chain segments in the films is also listed in Table 1 and has been

Table 1: Sample Overview and Thicknesses

Sample Name	β-phase (%)	t (nm)
Sample 1	0	131
Sample 2	ca 0	139
Sample 3	0.5	130
Sample 4	6.4	125
Sample 5	7.4	122
Sample 6	10.9	126
Sample 7	12.4	134
Sample 8	14.0	134
Sample 9	18.6	137
Sample 10	22.4	130
Sample 11	24.5	125
Sample 12	25.6	135

determined for each sample from the film thickness and absorption data (see Section 2 for the data and more details on the method).

To ensure the stability of the samples over the time span they were investigated, we performed photoluminescence (PL) measurements after each experiment. The spectral shape of the PL differs considerably with changing β-phase content (see Section 3) and we therefore consider this to be a good indication for conformational changes within the films that may have occurred over time. Sample 4 was partially damaged after the PLQE measurement. Consequently, no time-resolved could be measured for this sample.

In addition to the 12 samples presented above, the same method was used to fabricate samples with higher β-phase content. However, vol% of paraffin oil in excess of 0.75 vol% led to the fabrication of soft polymer films whose large surface roughness and poor consistencies made the films unsuitable for optical measurements. We attribute this threshold to a quantity of paraffin oil in solution large enough to hinder the spin-coating process. We found that an intermediate 13th sample with a β-phase content of 33.4% was the last sample to allow suitable measurements. While already showing a significant increase in thickness (161 nm) compared to the other twelve samples, it presented a surface of sufficient quality to still permit optical measurements. The measurements from this sample are in agreement with the overall trends for increasing β-phase content of the study; red-shift of the emission and absorption peak, lower Huang Rhys parameter, high PLQE (0.71), increase in radiative decay rate, slight increase in nonradiative decay rate (in line with the trend for the other samples of the series), rapid PL decay caused by the resonant energy transfer with a square-root dependence on time and a decrease in Förster radius determined from both, transient data and spectral overlap calculations.

2 Absorption Spectra and Determination of β-Phase Content

In this section we provide the experimental details of the absorption measurements and outline how we use these to determine the β-phase content of the PFO films.[4–6]

2.1 Experimental Details

We recorded absorption spectra with a dual-beam Shimadzu UV-2600 spectrophotometer equipped with a diffuse reflectivity (integrating sphere) attachment, allowing the absorption spectra to be corrected for reflection and scattering losses. Transmittance T, specular reflectance sR and diffuse reflectance dR were recorded over a wavelength range of 300 nm to 500 nm in steps of 1 nm. The absorptance A is obtained from the data as:

$$A = 1 - (T + sR + dR) = 1 - T - R_{tot}. \tag{1}$$

2.2 Absorptance Spectra

The resulting absorptance spectra are shown in Fig. 1. The absorptance spectra are considered to be a linear superposition of contributions from glassy phase and β-phase chain segments in the films. The disordered glassy phase chain segments contribute a broad absorption peak centered at around 380 nm, whereas the contribution of the on a molecular level more geometrically confined β-phase chain segments is manifested as a much narrower 0-0 peak around 430 nm followed by a vibronic progression.[7] At low β-phase content, the peak develops as a shoulder on the red edge of the total absorption and becomes more distinct with increasing β-phase content in the film.

2.3 β-Phase Fraction and Absorptance Spectra

The absorption data were used to determine the percentage of chain segments in β-phase conformation, $\beta_{fraction}$ and we will in the following give a brief derivation of the expression we used.[4–6] $\beta_{fraction}$ is defined as

$$\beta_{fraction} \;=\; \frac{c_\beta}{c_\beta + c_g}, \tag{2}$$

where c_β and c_g are the concentrations of the β-phase and glassy phase chain segments in the film, respectively. Concentration c and absorption are linked through the Beer-Lambert law, which is expressed in terms of the molar extinction coefficient $\epsilon(\lambda)$ and the sample thickness t as:

$$I(\lambda) \;=\; I_0(\lambda)\; 10^{-\epsilon(\lambda)\; c\; t}, \tag{3}$$

where $I_0(\lambda)$ and $I(\lambda)$ denote the intensities entering and leaving the film in the absorption experiment. The molar extinction coefficient $\epsilon(\lambda)$ is related to the (napierian) absorption coefficient $\alpha(\lambda)$:

$$\epsilon(\lambda) \;=\; \frac{\log_{10}(e)}{c}\; \alpha(\lambda), \tag{4}$$

which we obtain from the experimental data at each recorded wavelength λ as:

$$\alpha \;=\; -\frac{1}{t}\; \ln(\frac{T}{1 - R_{tot}}). \tag{5}$$

A spectral integration of the molar extinction coefficient over wavenumbers ν provides the oscillator strength f:

$$f \;=\; const \times \int \epsilon(\nu)\, d\nu \;= \frac{const'}{c} \times \int \alpha(\nu)\, d\nu \;=\; \frac{const'}{c} \times SA, \tag{6}$$

which is a measure of the strength of the electronic transition underlying the absorption process. SA denotes the spectral area and is by the above equation defined as $SA \;=\; \int \alpha(\nu)\, d\nu$.

Using the oscillator strength, we can rewrite the concentrations in Eq. 2 in terms of the spectrally integrated areas of the glassy phase and the β-phase chain segments $SA_{g,\beta}$ and $f_{g,\beta}$. The constant term from Eq 6 cancels out and by expanding the equation with f_β we arrive at the following expression for the β-phase fraction:

$$\beta_{fraction} \;=\; \frac{SA_\beta}{\frac{f_\beta}{f_g} \times SA_g + SA_\beta}. \tag{7}$$

The oscillator strengths of the glassy phase and β-phase chain segments differ in value. Their ratio has been derived by Huang et al.[5] using time-dependent density functional theory to be $\frac{f_\beta}{f_g} \;=\; 1.08$, which we use here.

Therefore, in order to obtain the fraction of β-phase chain segments for each film, the contributions of the glassy phase and of the β-phase chain segments to the total absorption of the film need to be separated. This is achieved by scaling the absorption spectrum of a glassy film with comparable thickness (termed "glassy equivalent", abbreviated "ge") to the total absorption spectrum of the investigated film at wavelengths below 350 nm. In the wavelength range of 300 nm to 350 nm, the contribution of β-phase chain segments to the total absorption has been found to be negligible.[7,8] We assume that the total absorption in this wavelength range only stems from glassy phase chain segments and that each glassy chain absorbs the same amount of energy. We introduce a scaling factor F and can write the following equations for the absorption coefficients:

$$\alpha_{ge} \;=\; \alpha_g \times (1 - F) \tag{8}$$

$$\alpha_{tot}^{300-350} \;=\; \alpha_g^{300-350} \times (1 - F), \tag{9}$$

where α_g, α_{ge} and α_{tot} denote the glassy, glassy equivalent and total-absorption coefficients and the superscript in Eq. 9 refers to the wavelength range in which the equation holds. We fit Eq. 9 to the absorption data in the wavelength range from 300 nm to 350 nm to obtain

the scaling factor F. We further determine the "glassy spectral area" SA_g from Eq. 8 and the definition of SA. The "β-phase spectral area" SA_β is determined by subtraction of SA_g from the total spectral area. We then use Eq. 2 to determine the β-phase fraction for each film. The resulting values are given in Table 1. The total absorptance spectrum and the contributions from the glassy and β-phase are shown in Fig. 3 for each β-phase containing sample individually. The β-phase absorptance as a function of β-phase percentage in the film is depicted in Fig. 2.

The β-phase main-peak dispersal ranges from 425 nm to 433 nm, showing a red-shift (towards higher wavelengths) with increasing β-phase content. This observation is discussed in Section 3. Compared to other studies,[2,4] the main peak of the β-phase absorptance is slightly blue-shifted and the resolution of the vibronic progression and the appearance of the β-phase peak in the total absorption are seen at higher β-phase contents only. This could be caused by the blue-shift of the peak, as there is more overlap with the broad glassy absorption peak at lower wavelengths. In comparison with the PL spectra, the absorption spectra appear to be broader, in particular beyond the 0-0 peak. The origin of this might be related to the method used for determining the β-phase absorptance spectrum (as outlined above), relying on the subtraction of the "glassy equivalent" absorptance spectrum from the total absorptance of a film containing some β-phase. If the "glassy equivalent" absorptance spectrum does not fully accurately represent the actual glassy phase absorption in the film containing some β-phase, the subtraction of this spectrum may lead to slight distortions in the resulting β-phase spectrum. There are two possible reasons for this to be the case. First, polymer chains in a particular conformation or local environment may be more likely to convert to β-phase, which means that the sub-set of unconverted glassy phase chains left differs from the ensemble found in an all glassy film. Second, the presence of β-phase in the film might introduce strain on the glassy phase, slightly shifting its energetic landscape. Given the dependence of β-phase presence on strain and local order, both of these scenarios

are plausible. Such differences would be most prominent at the onset of the glassy phase absorption, where changes in energetic disorder will lead to a sharpening or broadening of the onset. For the calculation of the Frster radii (see Section 6.2), we determine the spectral overlap between glassy phase emission and β-phase absorption, which however mostly includes the 0-0 peak of the β-phase absorption, which is sufficiently red-shifted from the absorption onset of the glassy phase. Additionally, the spectral deconvolution method might introduce a small inaccuracy on the β-phase percentage. However, the trend of increasing β-phase percentage is very clear and small deviations will not change any of the discussions and conclusions we present.

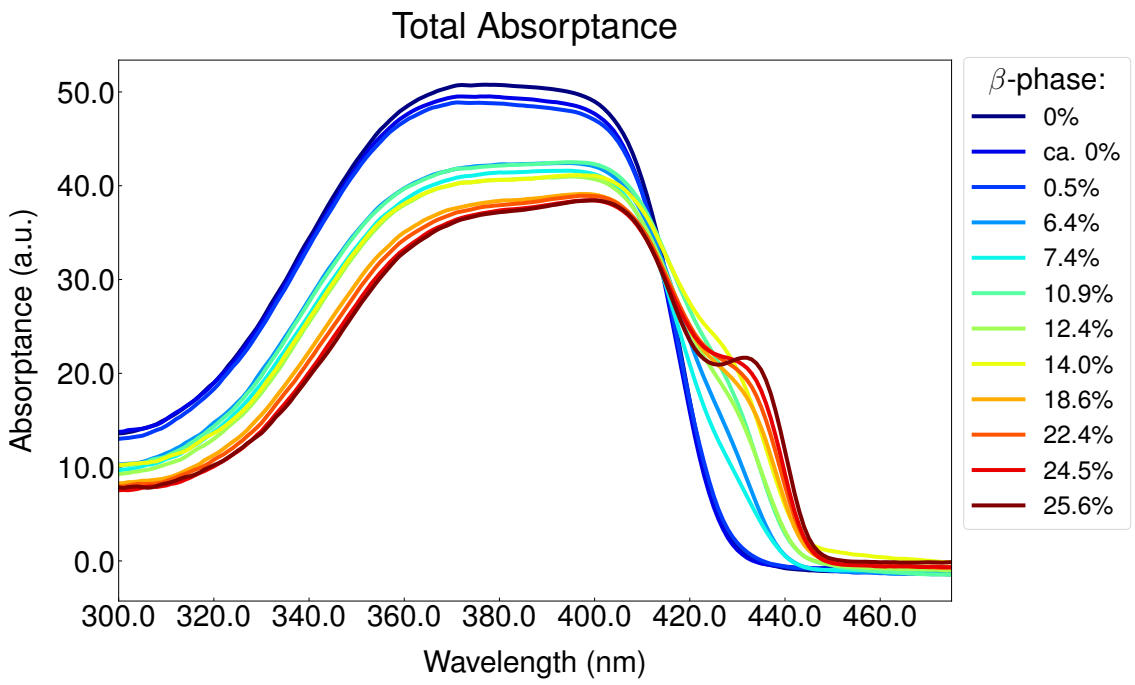

Figure 1: Absorptance spectra for all films. The spectra are a superposition of contributions from the glassy and β-phase chain segments. The spectra are corrected for spectral and diffuse reflectance.

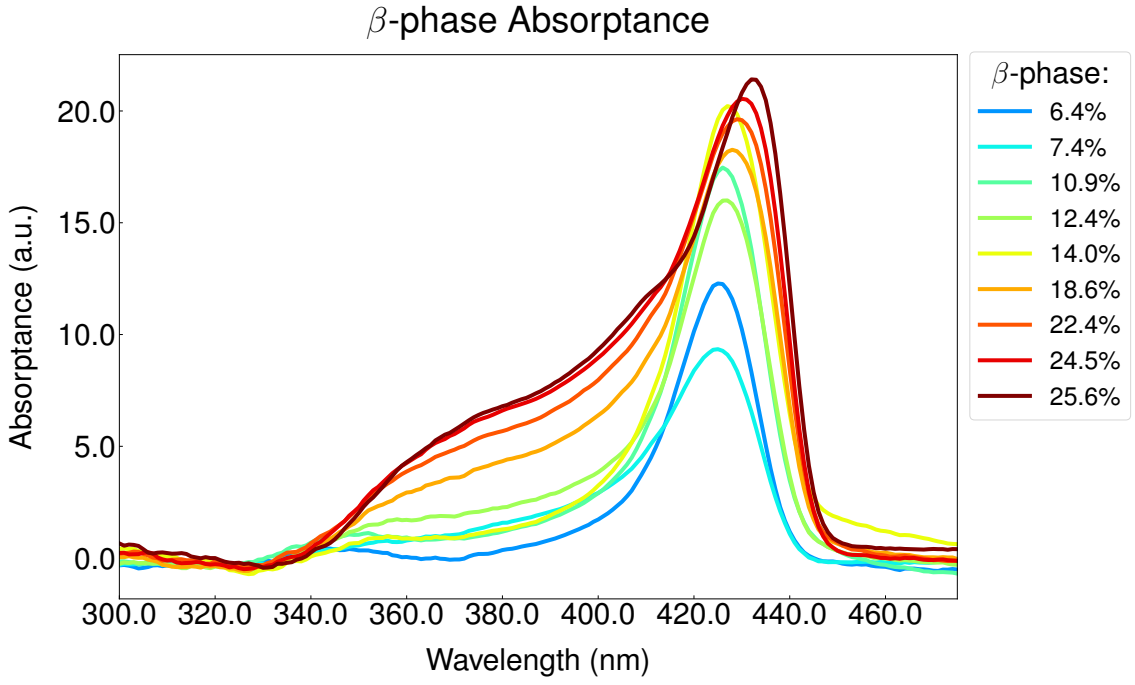

Figure 2: β-phase absorptance spectra of the films containing some ($\geq 6.4\%$) β-phase chain segments. The spectra were obtained by subtraction of the contribution of the glassy chain segments from the total absorptance, using the fitting method described in the text.

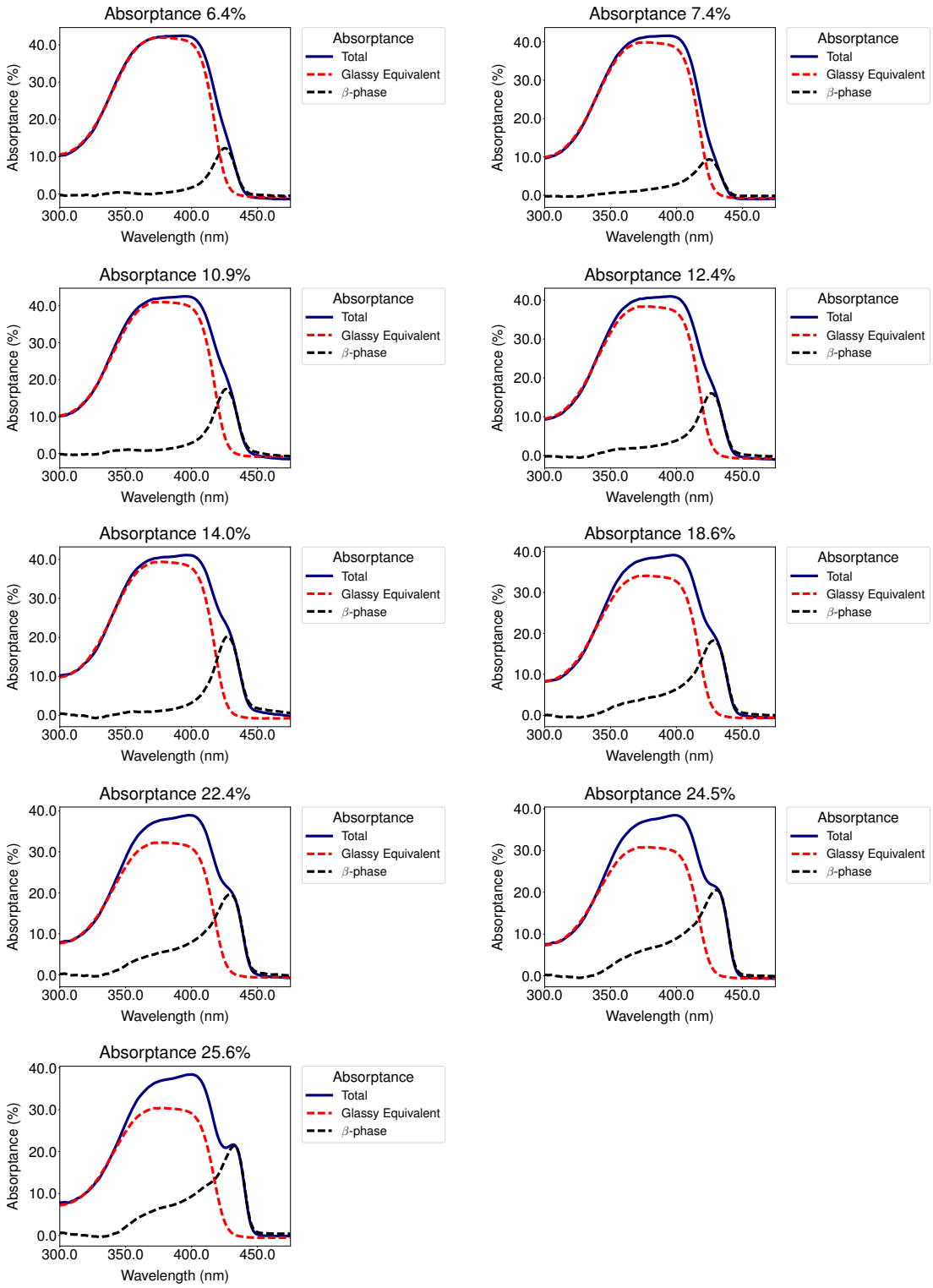

Figure 3: Total absorptance spectra (blue) and contributions of the glassyphase (red) and of the β-phase (black). The decomposition procedure is described in the main text of the SI. The spectra are presented for each sample containing some ($\geq 6.4\%$) β-phase. The β-phase content of the sample is indicated in the respective heading.

3 Time-Integrated Photoluminescence Spectra

In this section, we outline the experimental details and provide additional analysis of our PL measurements in support of the discussion of Fig. 1 in the main text.

3.1 Experimental Details

We measured time-integrated PL spectra for all samples using a monochromator (Jobin Yvon: Triax 190) and a nitrogen-cooled charge coupled device (CCD) silicon detector (Jobin Yvon: Symphony). The samples were kept under vacuum and were excited at a wavelength of 380 nm with a power of 4 µW, an excitation spot area of roughly 0.1 mm^2 and we used an integration time of 3 s. The spectra are corrected for the instrumental response of the system.

3.2 PL Peak Position

The normalized PL spectra are shown in Fig. 1a. The PL spectra of the films containing zero to very low ($\leq 0.5\%$) β-phase (henceforth called "glassy films") feature vibronic peaks located at 426 nm, 451 nm and 480 nm. The films containing some ($\geq 6.4\%$) β-phase chain segments show emission peaks around wavelengths of 437 nm, 465 nm and 496 nm. The peaks red-shift with increasing β-phase content. The shift is further quantified in Fig. 4, which also shows that the shift occurs not only for the 0-0 but also for the 0-1 vibronic peak, ruling out self-absorption as the main cause of the shift (see Fig. 1 for the absorption spectra).

3.3 Peak Narrowing

In addition to the shift in peak position, the PL peaks become spectrally narrower with increasing β-phase content. Fig. 5 shows the averaged FWHM (full width at half maximum) of the 0-0 peak and the 0-1 peak as a function of β-phase variation. These data were acquired by fitting a sum of Gaussian peak profiles to each of the peaks. As the inset of Fig. 5 shows,

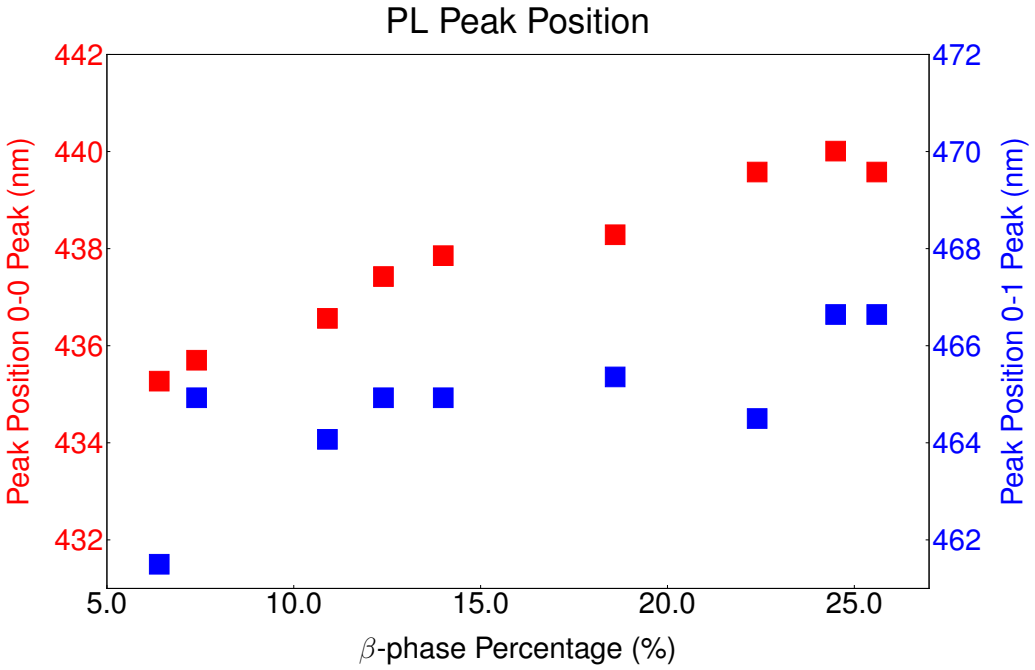

Figure 4: Position of the β-phase PL peaks (0-0 peak in red, 0-1 peak in blue) as a function of β-phase percentage. Both peaks show a red-shift with increasing β-phase percentage.

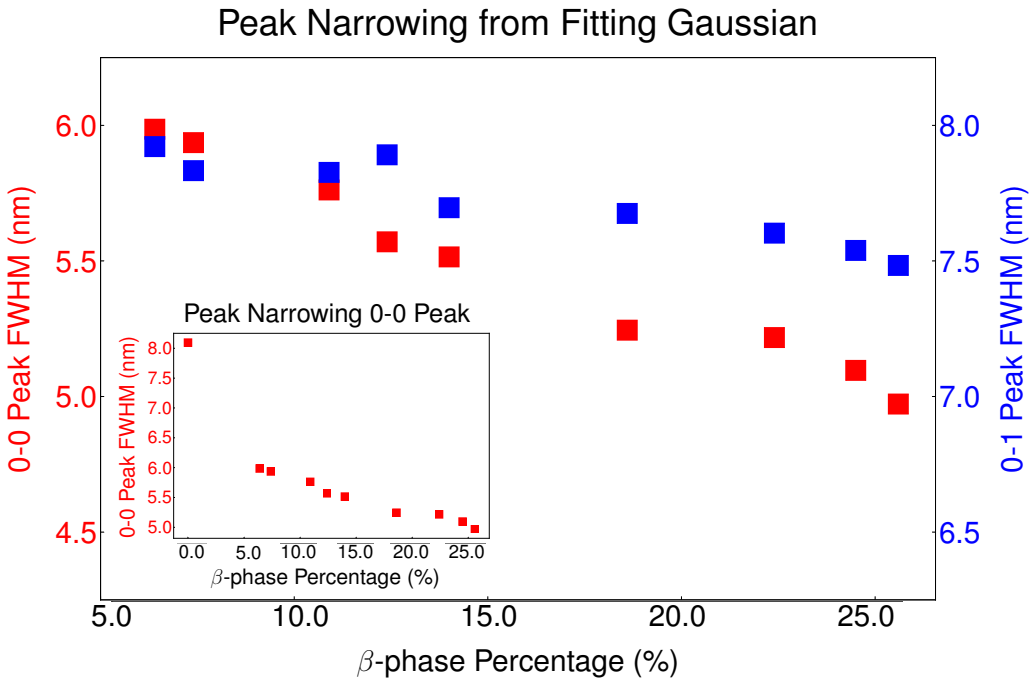

Figure 5: FWHM of the β-phase 0-0 (red) and 0-1 (blue) PL peaks as a function of β-phase percentage, obtained by fitting of a sum of Gaussian peak profiles to each peak. Both peaks narrow with increasing β-phase percentage. The insert shows the peak width of the 0-0 peak including the glassy film.

the 0-0 peak of the glassy films is much broader than the 0-0 peak of the β-phase films. The 0-0 peak of the glassy samples stems from emission from disordered chain segments and is therefore by the same argumentation as above expected to be broader than the 0-0 peak of the β-phase films, which stems from emission from the geometrically more rigid β-phase chain segments. Again, observing the narrowing not only for the 0-0 but also the 0-1 peak indicates that the peak narrowing with increasing β-phase content is not mainly caused by self-absorption.

3.4 Huang-Rhys Parameter

The Huang-Phys Paramenter S is related to the conformational relaxation energy in the excited state. It can be seen as a measure of geometric reorganization energy upon an electronic transition ($S \propto \Delta Q^2$, the square of the displacement in conjugation coordinate).[9] The parameter can be assessed as $S = \frac{I_{0-1}}{I_{0-0}}$ from the ratio of the peak intensities I_{0-1} and I_{0-1} of the 0-0 and 0-1 transitions, which are associated with the C-C stretch vibration replica.

We have deduced the Huang-Rhys parameter for each sample from the intensity ratio of the 0-0 and 0-1 PL peaks, which were graphically extracted from Fig 1a of the main manuscript. At low temperatures the 0-1 peak is known to consist of two spectrally overlapping peaks.[10] However, at higher temperatures, only one peak can be observed and as they are no longer distinguishable this does not change the trend we discuss here. The Huang-Rhys parameter (shown in Fig. 1c of the main manuscript) decreases with increasing β-phase content (discussion in main manuscript).

4 Photoluminescence Quantum Efficiency

4.1 Experimental Details

We measured PLQE using a Jobin Yvon Horiba Fluoromax 4 spectrofluorometer equipped with a diffusely reflecting integrating sphere (Quanta-phi). We used an excitation wavelength of 390 nm. The experimental and calculation methods used here were identical to the ones presented in Ref. 4.

5 Lifetimes and Decay Rates

5.1 Experimental Details

The PL lifetimes and decay rates were determined by time correlated single-photon counting (TCSPC) using a single-photon avalanche diode detector, which allows for a time-resolution of 40 ps.[11] The samples were excited at a wavelength of 405 nm (glassy sample) or 432 nm (samples containing some β-phase, further discussion below) at a power of 200 µW and an excitation spot area of roughly 0.1 mm^2. The excitation decay was observed at 425 nm (for the excitation at 405 nm only), 438 nm, 450 nm and 464 nm. The samples were kept under vacuum during the experiment.

Emission from samples containing β-phase (even a small amount) stems overwhelmingly from β-phase chain segments, regardless of the excitation wavelength, because the transfer of excitation energy from glassy phase to β-phase chain segments is ultrafast and complete. This conclusion is experimentally supported by the observed dominance of β-phase spectral features in the time-integrated PL (see Fig. 1a of the main manuscript) and the ultra-fast (picoseconds time scale) energy transfer, which is completed before significant photon emission has occurred. Therefore, the β-phase can be excited in two ways: 1. direct excitation (at 432 nm) and 2. excitation through energy transfer from the glassy phase chain segments (at 405 nm). Both excitation wavelengths should yield the same PL-lifetimes. Analyzing the data, we initially found a slight disagreement in lifetimes for the two excitation wavelengths. However, this discrepancy was resolved upon illuminating some of the samples alternatively from the back through the quartz substrate. On these samples we performed 4 measurements for each detection wavelength: exciting at 405 nm and 432 nm from the front as well as through the back. In doing so, we found that the PL lifetimes for 1. 432 nm front illumination, 2. 405 nm back illumination and 3. 432 nm back illumination yield the same results for PL lifetimes and only the 405 nm front illumination results in slightly different PL lifetimes. On the basis of this result, we attribute the observed differences in PL lifetimes

from front and back illumination at 405 nm to the presence of impurities/traps at the surface of the PFO films. At the wavelength of 405 nm the penetration depth is shorter than at 432 nm, making the 405 nm excitation more prone to surface impurities. No difference in PL lifetimes was observed when illuminating the samples at 432 nm from front and back and we therefore chose the excitation wavelength to be 432 nm (direct excitation of β-phase) for further analysis and excited the samples from the front. For all measurements, the detection wavelength does not alter the resulting PL lifetime, which can be seen in Fig. 6, showing the decay rates obtained from different detection wavelengths, as well as an average decay rate over all detection wavelengths. The decay rates presented here are obtained by averaging over all detection wavelengths.

In order to extract the natural lifetimes τ, a single exponential time decay $e^{-(t-t_0)/\tau}$ is fitted to the measurement data from 0.5 ns to 2 ns, where t_0 is chosen for each sample to be at 50% signal strength in the rise of signal upon excitation. Exemplary fits are shown for all samples in Fig. 7 for a detection wavelength of 450 nm.

From the lifetimes τ, the total, radiative and nonradiative decay rates k_{tot}, k_{rad} and k_{nonrad} are calculated for each sample using the following set of relations:

$$\begin{aligned} k_{tot} &= 1/\tau \\ k_{tot} &= k_{rad} + k_{nonrad} \\ k_{rad} &= PLQE \times k_{tot}. \end{aligned} \tag{10}$$

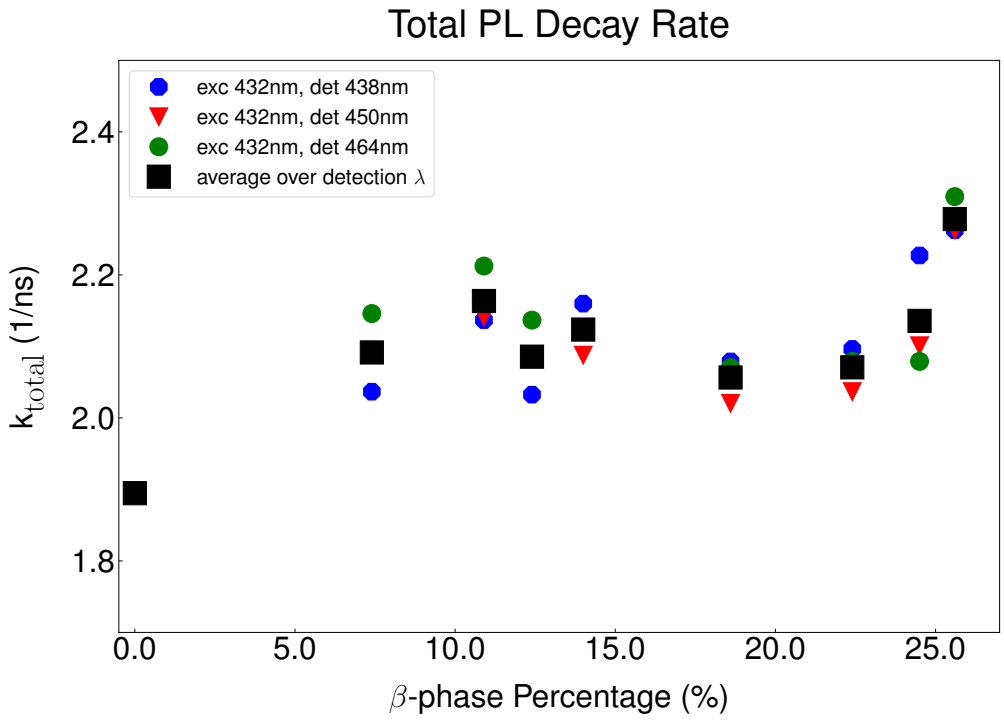

Figure 6: Total decay rate for each sample obtained by a mono-exponential fit to TCSPC data. The rates calculated for the different detection wavelengths and an average over these wavelengths are shown.

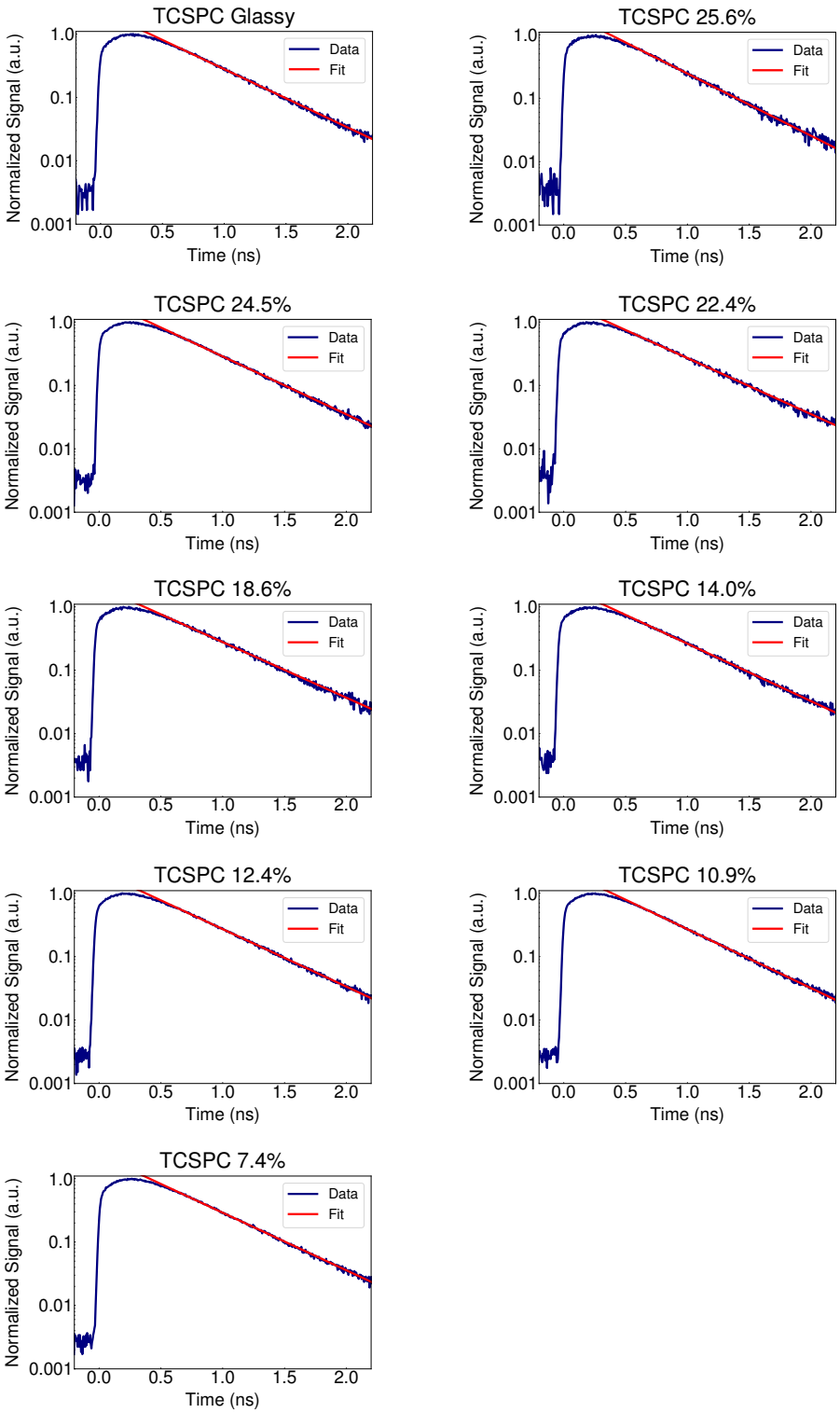

Figure 7: Experimentally determined PL lifetime decay (blue) and mono-exponential fits (red, fitted to 0.5 ns to 2 ns). The β-phase content of each sample is indicated in the respective heading. The lifetime decay was measured at 450 nm.

6 Förster Radii

Förster resonant energy transfer is based on dipole-dipole interactions between an energy donor (here, glassy phase chain segments) and an energy acceptor (here, β-phase chain segments). It is used to express the rate of energy transfer in terms of the Förster radius R_0, which is defined as the distance between donor and acceptor at which excitation energy transfer from the donor to the acceptor is as likely to happen as any other de-excitation of the donor.[12,13] The Förster radius can be obtained in several ways.[14] We determined the Förster radius from i) time-resolved PL decay (Section 6.1) and ii) the spectral overlap between donor emission and acceptor absorption (Section 6.2). The primary discussion of our results can be found in the main article. We will in this section provide additional derivations and background on using Förster theory as well as information on the experimental details.

6.1 Calculation of Förster Radius from PL Dynamics

6.1.1 Experimental Details

Up-conversion spectroscopy enables ultrafast measurement of PL with a femtoseconds range time-resolution, allowing experimental investigation of fast energy transfer dynamics.[15–17] The technique is based on frequency mixing in a non-linear dielectric material (optical gating).[18,19] All samples were excited at 405 nm with an excitation pulse generated by a mode-locked Ti:Sapphire laser at a repetition rate of 80 MHz, having a pulse duration of 80 fs and an excitation spot area of roughly 0.1 mm^2. The subsequently emitted PL was collected and spatially and temporally overlapped with a synchronous "gate" beam within a beta-barium-boronate (BBO) crystal. Sum-frequency ("up-converted") photons are created only when the gate and PL pulses are simultaneously incident on the BBO crystal. The gate beam therefore acts as a temporal pass gate to the PL in the experiment. The up-converted signal was collected and dispersed in a monochromator. Finally, the signal was detected by a nitrogen-cooled CCD silicon detector, which was set to detect the signal stemming from sample PL

at 419 nm, of which the main contribution is expected to be attributed to the PL-decay of the glassy phase.[15] The samples were kept under vacuum to avoid photo-oxidation. For each sample, four decay traces were consecutively recorded, with the time delay swept forwards for the first and third measurement and backwards for the second and forth measurement to monitor and ensure sample stability during experimentation. The fundamental limit of the time-resolution of the upconversion-system is the pulse duration. However, there will be temporal broadening due the finite width of the non-linear crystal used for "up-converting" the signal, which causes the group velocity to disperse.[20] Our upconversion system has a time-resolution of approximately 300 fs. The averaged and normalized traces are depicted in Fig. 2 of the main manuscript.

6.1.2 Calculation of the Förster Radius

The time-resolved PL data can be used for deduction of the Förster Radius R_0. The expression for R_0 is derived by considering an ensemble of donors and acceptors, which are assumed to be evenly distributed in space. An average is taken over all possible energy transfers from a donor to an acceptor, assuming that the energy transfer is governed by dipole-dipole interactions[6,12,16,21,22] (more detailed derivation below):

$$R_0 \;=\; \left(\frac{3}{2\pi^{\frac{3}{2}}} \, \frac{\sqrt{\tau_d}\gamma}{c_\beta} \right)^{1/3} \tag{11}$$

where τ_d denotes the excitation lifetime of the donor, here the glassy phase chain segments, γ relates the Förster radius to the donor emission and is determined from PL-upconversion (see Eq. 29) and c_β is the density of β-phase chromophores.

Excitation lifetime of the glassy phase chromophores, τ_d: We determined τ_d by TCSPC (see Section 5) to be 526 ps. This lifetime represents the total lifetime rather than the radiative lifetime only.

Analysis of the PL-upconversion transients, γ: A brief derivation of the equations used for the analysis of the PL-upconversion data is given below, based on Refs. 12, 16, 22–24: If interactions between the excitations can be neglected (low density regime), the following rate equations for the number of excited donors/acceptors $n_{d/a}$ characterize the energy transfer dynamics:

$$\frac{dn_d}{dt} = G_d(t) - \frac{1}{\tau_d} n_d(t) - k_{da}(t) n_d(t) \tag{12}$$

$$\frac{dn_a}{dt} = G_a(t) + k_{da}(t) n_d(t) - \frac{1}{\tau_a} n_a(t). \tag{13}$$

Here, $G_d(t)$ represents the direct excitation rate of the donors and $G_a(t)$ refers to direct excitation of acceptor molecules, $\tau_{d/a}$ are the excitation lifetimes of the donor/acceptor and $k_{da}(t)$ is the energy transfer rate. The rate equations as presented in Eqs. 12 and 13 hold for energy transfer from a donor to an acceptor ensemble. The nature of the energy transfer determines the transfer rate $k_{da}(t)$. For Förster-type resonant energy transfer, which assumes that the energy transfer is governed by dipole-dipole interactions, and in the case of an even spatial distribution of the acceptors in 3 dimensions we can write:[16,22]

$$k_{da}(t) = \frac{\gamma}{\sqrt{t}}, \tag{14}$$

with

$$\gamma = \frac{2\pi^{\frac{3}{2}}}{3} \frac{c_a}{\sqrt{\tau_d}} R_0^3. \tag{15}$$

Here, c_a denotes the acceptor concentration and R_0 is the Förster radius. Using the initial conditions $G_{d/a}(t) = N_{d/a}\,\delta(0)$ (delta-like excitation at $t = 0$) and $n_{d/a}(0) = 0$ (no excited donors/acceptors at $t = 0$) the rate equations are solved by:

$$n_d = N_d \exp(\frac{-t}{\tau_d} - 2\gamma\sqrt{t}) \tag{16}$$

$$n_a = \bar{N_a} \{\Psi(\frac{\gamma}{\vartheta} + \vartheta\sqrt{t}) - \Psi(\frac{\gamma}{\vartheta})\} \exp(\frac{-t}{\tau_a}), \tag{17}$$

where we have introduced,

$$\vartheta \;=\; \sqrt{|\tau_d^{-1} - \tau_a^{-1}|}, \tag{18}$$

$$\bar{N_a} \;=\; N_a \;+\; N_d\,\sqrt{(}\pi)\,\frac{\gamma}{\vartheta}\exp(\frac{\gamma}{\vartheta})^2 \tag{19}$$

and $\Psi(x)$ denotes the error function:

$$\Psi(x) \;=\; \frac{2}{\sqrt{\pi}}\int_0^x e^{-y^2}\,dy. \tag{20}$$

We model the PL intensity data as a sum of contributions from both, glassy phase and β-phase chain segments:

$$I_{PL} \;=\; C_d\,n_d \;+\; C_a\,n_a, \tag{21}$$

where in addition to the excited donor/acceptor populations $n_{d/a}$, the excitation and detection wavelengths influence the strength of the contributions to the PL intensity (accounted for by C_d and C_a) from each of the two phases. Khan et al.[15] have argued that at 419 nm the β-phase emission is negligible. However, from our emission data (Fig. 1a of the main manuscript), we expect a non-negligible but small contribution from the β-phase chain segments. Direct excitation of the acceptor molecules is often neglected, based on a small acceptor concentration or the acceptor not absorbing at the excitation wavelength. In our case, there is a considerable amount of acceptors (β-phase chain segments) present in the film, which absorb at 405 nm, which is why we include direct excitation of the acceptors in the derivation, although we still expect this contribution to be small. In order to derive an expression for $I_{PL}(t)$, we note that $\tau_{d,a} >> t$ over the timescales t of our energy transfer measurements, because the excitation lifetime of the donor (glassy phase) and the acceptor (β-phase) are of the order of ns, whereas the energy transfer dynamics are investigated on a ps timescale. Mathematically we can therefore assume $\tau_{d,a} \to \infty$, we and rewrite Eqs. 12,

13 as:

$$\frac{dn_d}{dt} \;=\; G_d(t) \;-\; k_{da}(t)n_d(t) \tag{22}$$

$$\frac{dn_a}{dt} \;=\; G_a(t) \;+\; k_{da}(t)n_d(t). \tag{23}$$

Adding these two equations, we find

$$\frac{dn_d}{dt} \;+\; \frac{dn_a}{dt} \;=\; G_d(t) \;+\; G_a(t) \tag{24}$$

and for $t > 0$

$$\frac{dn_d}{dt} \;+\; \frac{dn_a}{dt} \;=\; 0, \tag{25}$$

which is solved by

$$n_d(t) \;+\; n_a(t) \;=\; \text{const}, \tag{26}$$

implying that the total number of excited donors plus excited acceptors does not change over time, which is to be expected as we are assuming that there are no decay pathways for the excitation ($\tau_{d,a} \to \infty$) other than transferring from the donor to the acceptor. Using the initial conditions, this also implies const $=\; N_d \;+ N_a$. Eqs. 22, 23, 26, are thus solved by:

$$n_d \;=\; N_d \exp(\text{-}2\gamma\sqrt{t}) \tag{27}$$

$$n_a \;=\; N_a \;+\; N_d\,(1 - \exp(\text{-}2\gamma\sqrt{t})) \tag{28}$$

and the total PL intensity $I_{PL}(t)$ then takes the following form:

$$I_{PL}(t) \;=\; A \exp(\text{-}2\gamma\sqrt{t}) \;+\; B, \tag{29}$$

where $A \;=\; (C_d - C_a)\,N_d$ and $B \;=\; C_a\,(N_d + N_a)$. Eq. 29 was fitted to the transient data to obtain γ, A and B. For sample 5 (7.4%), the amplitude A was limited to obtain a sensible

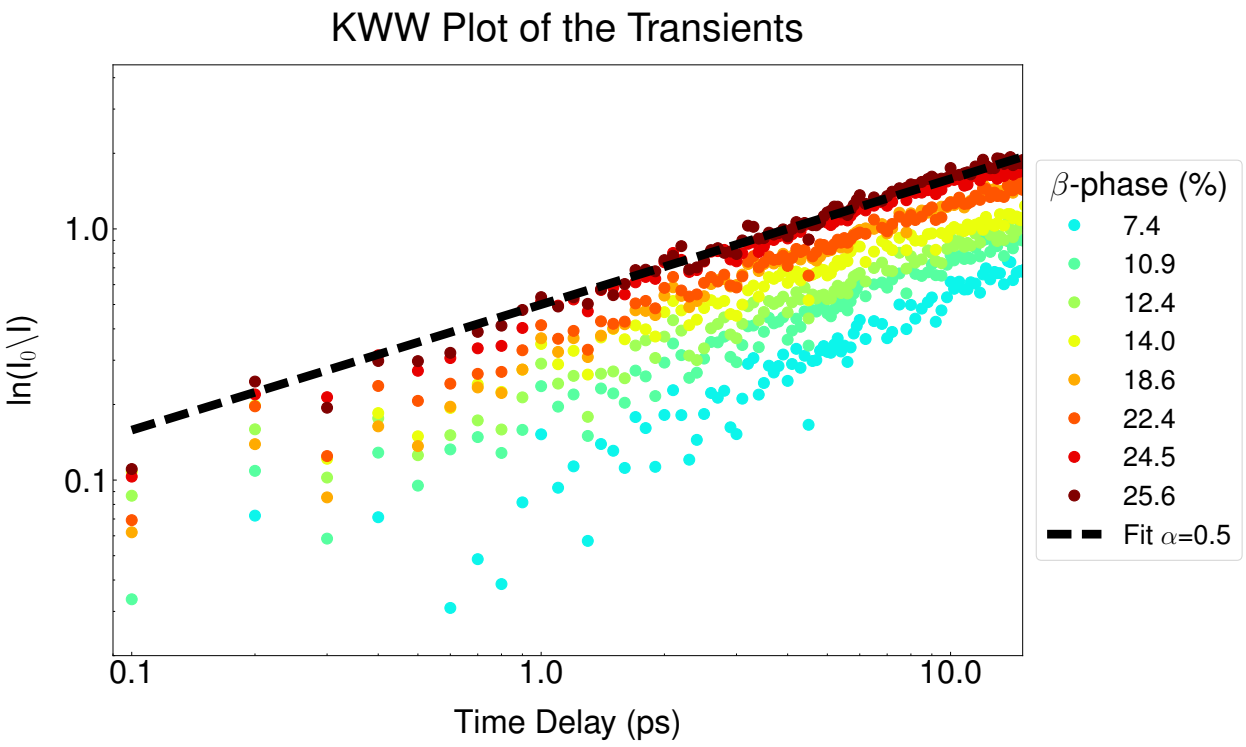

Figure 8: KWW plot of the PL-upconversion transient data with the constant offset I_β^0 subtracted from it. The colors indicate the β-phase percentage in the film. A line with slope $\alpha = 0.5$ is fitted to the data.

fit (see discussion in Section 6.1.3). The fits for each sample, together with the data, are displayed in Fig. 9, showing that the experimental data can be well described using Eq. 29.

To provide further argumentation for using Förster theory and therefore the $\sqrt{t}$-term in Eq. 29, we plotted the transient data (subtracting the constant offset B) in a Kohlrausch-Williams-Watts (KWW) representation in Fig. 8. In a KWW representation, the logarithm of the ratio of the initial PL intensity I_{PL}^0 and the PL intensity $I_{PL}(t)$ is plotted versus time on a log-log scale.[25] We assume the PL intensity, representing the surviving exciton population at a time t and therefore the excitation decay, to follow a power law:

$$I(t) \;=\; I_0 \; e^{(-t/t_0)^\alpha} \tag{30}$$

The slope in Fig. 8 thus represents the value for the exponent α. A slope of $\alpha = 0.5$ fits the data well, supporting the $\sqrt{t}$ fit and therefore the use of Förster theory for the analysis.

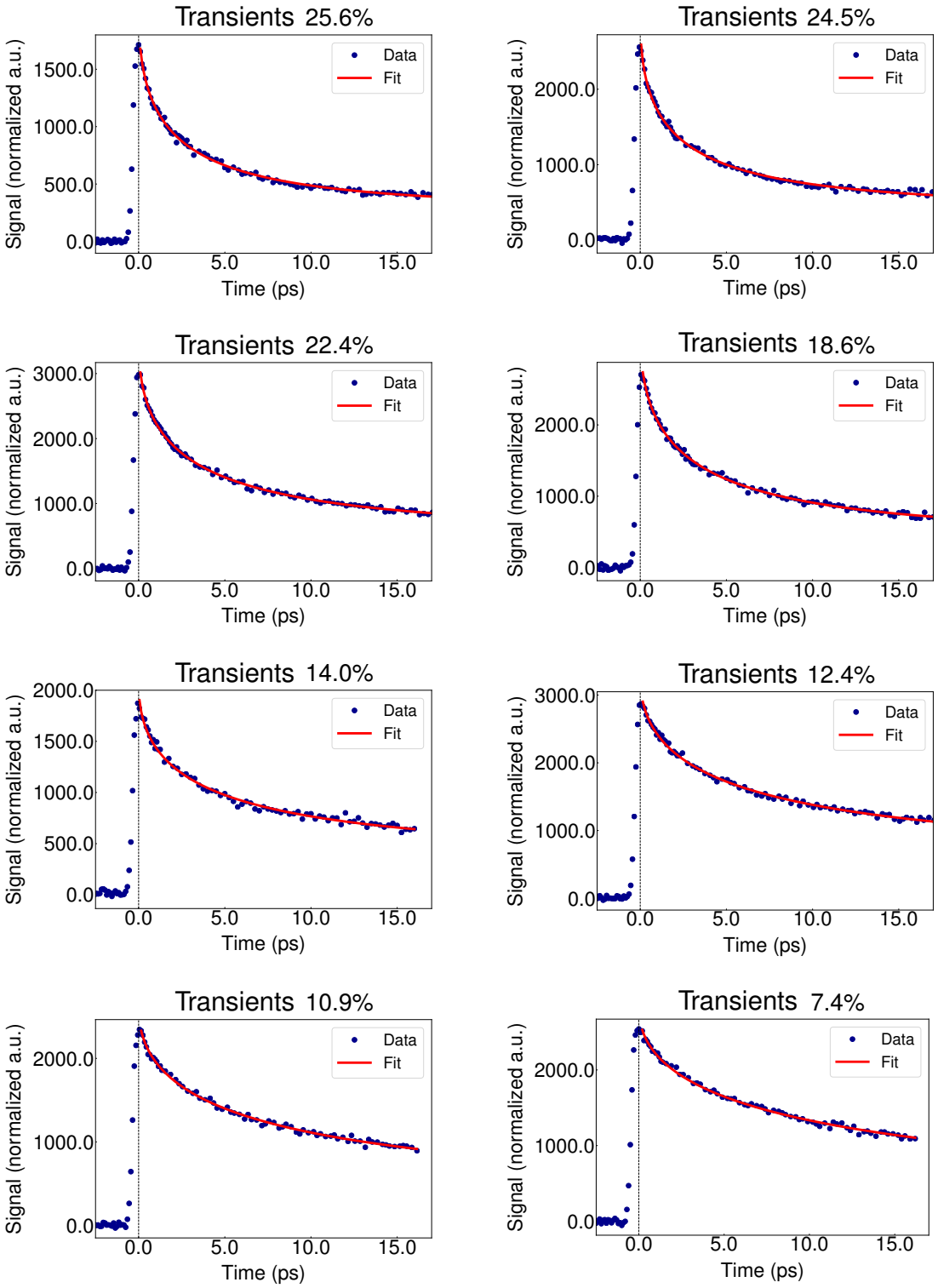

Figure 9: PL-upconversion transients for each measured sample (β-phase content indicated in respective header): Experimental data in blue and a fit of Eq. 29 to the data in red.

Density of β-phase chromophores, c_β: The β-phase chromophoremdensity is estimated as (see Eq. 2):

$$c_\beta \;=\; \frac{\beta_{fraction}}{1-\beta_{fraction}}\; c_g, \tag{31}$$

where $\beta_{fraction}$ denotes the fraction of total chromophores in β-phase, which has been determined from absorption data (see Section 2) and c_g is the chromophore density in glassy spun-cast film, which was determined by Stevens et al. to be $2 \times 10^{19}\,\mathrm{cm}^{-3}$.[26] Other authors[15] have at this point also introduced a factor to account for the changes in chromophore density in an all glassy film compared to a film containing some β-phase chromophores. However, this is already incorporated into our initial calculation, as we take a change in glassy chromophore numbers into account when calculating the fraction of β-phase chromophores.

6.1.3 Results from Time-Resolved Data

To examine whether our fits are sensible, we investigated the ratio of the fitting parameters A and B (Fig. 10), defined through Eq. 29. A rough estimate of B/A can be done from absorption and PL spectra. The absorption spectra reflect how much of the initial excitation is absorbed by glassy phase and by β-phase chain segments (N_a and N_d) at the excitation wavelength. Fig. 2 shows that the higher the β-phase fraction the more is absorbed by β-phase chain segments, leading to an increase in B/A. The PL spectra contain information on C_a and C_g. Due to the red-shift in PL, C_a decreases with increasing β-phase, leading to a decrease in B/A. The effects from changes in PL and absorption spectra with varying β-phase fraction on B/A therefore compete. We performed a rough estimate of B/A from the absorption and PL spectra and found that the estimated values indeed agree with the range of values in Fig. 10. Only for sample 5 (7.4%), the amplitude A was limited to a realistic maximum value during the fitting process to obtain a sensible value for B/A.

The resulting Förster radii are noted in Table 2. We find a decreasing trend with increasing β-phase percentage. The magnitude of our R_0 values obtained from transient data is in agreement with the work of Khan et al.,[15] who determined $R_0 = 8.2 \pm 0.6\,\mathrm{nm}$ from

PL-transients for one sample containing roughly 25% β-phase, using however a different sample preparation method and a different method to estimate the β-phase content and the chromophore densities.

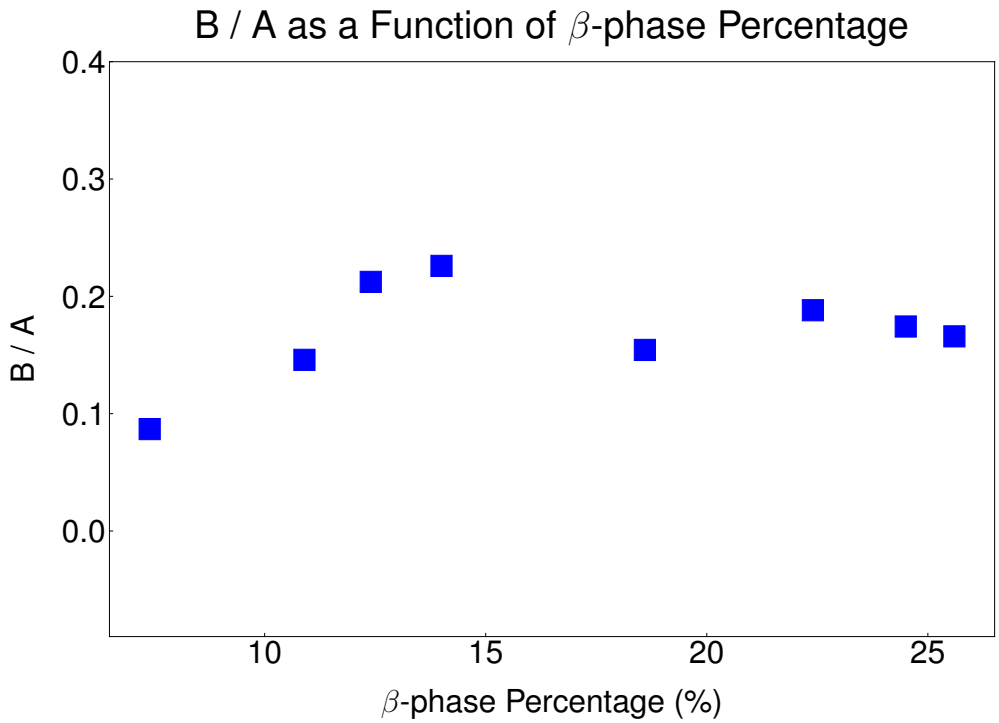

Figure 10: The fitting parameters B/A obtained from fitting Eq. 29 to the transient data (Fig. 2a of the main manuscript).

Table 2: Förster Radii from PL Transients obtained by Eq. 11.

β-phase (%)	R_0 (nm)
7.4	8.05
10.9	7.54
12.4	7.47
14.0	7.63
18.6	7.29
22.4	6.67
24.5	6.82
25.6	6.74

6.2 Calculation of Förster Radius from Donor Emission and Acceptor Absorption Spectra

A second way of calculating the Förster radius is from donor emission and acceptor absorption spectra. The experimental details and the spectra are presented in Sections 2 and 3.

6.2.1 Calculation of the Förster Radius

The following expression was used to estimate R_0:[9,14,27]

$$R_0 \;=\; \left(\frac{9\;\ln(10)\;\kappa^2\;\phi_d}{128\;\pi^5\;N_A\;n^4}\int I_d(\lambda)\epsilon_a(\lambda)\lambda^4 d\lambda\right)^{1/6} \;=\; 0.02108\;\left(\kappa^2\;\phi_d\;n^{-4}\;J\right)^{1/6}, \qquad (32)$$

where N_A is Avogadro's constant, κ denotes the geometric orientation factor of the donor and acceptor dipoles, ϕ_d is the PLQE of the glassy sample, n the refractive index and J is the overlap integral between donor (glassy phase chain segments) emission dynamics and acceptor (β-phase chain segments) absorption spectra in units of $\frac{\mathrm{dm^3 nm^4}}{\mathrm{mol\,cm}}$ in order to obtain R_0 in nm.

Geometric orientation factor κ: κ accounts for the relative geometric orientation of the donor and the acceptor dipoles:

$$\kappa = \vec{\mu_d}\cdot\vec{\mu_a} - 3(\vec{\mu_d}\cdot\vec{R_{da}})(\vec{\mu_a}\cdot\vec{R_{da}}), \qquad (33)$$

where $\vec{R_{da}}$ denotes unit vector of the the donor-acceptor separation, $\vec{\mu_a}$ and $\vec{\mu_d}$ are the normalized transition dipole moments of the acceptor and donor respectively. κ takes values ranging from 0 for mutually perpendicular arrangement to 2 for collinear alignment.[9] In our initial calculation, we used $\kappa = 0.845 \times \sqrt{2/3}$, which corresponds to a random, but fixed orientation of donors and acceptors randomly placed in the film.[16,28,29] The choice of κ is further discussed in the main article.

PLQE, ϕ_d: Including the PLQE of the glassy sample in the expression for R_0 and using the total lifetime when calculating the Förster radii from PL-dynamics in Eq. 11 ensures that the results are comparable. This means that the Förster radius is referring to the distance at which energy transfer is as likely to occur as any other de-excitation of the donor (as opposed to the distance at which energy transfer is as likely to happen as any other radiative de-excitation, which is sometimes used for the calculation of the Förster radius and is termed "effective Förster radius").

Refractive index, n: We assumed the PFO films to have a refractive index of $n_{eff} = 1.6$, which is a typical value for π-conjugated polymers.[30–34] This factor is kept constant for all samples and therefore does not influence any observed trends.

Overlap integral, J: J describes the overlap of the normalized donor fluorescence I_d and the molar extinction coefficient ϵ_a of the acceptor, which is linked to its absorption:[9,14]

$$J \;=\; \int I_d(\lambda)\epsilon_a(\lambda)\lambda^4 d\lambda. \tag{34}$$

In order to obtain I_d, the fluorescence spectrum of the glassy sample (see Section 3) was normalized to the integrated area below the emission curve. This was achieved by using a spline-interpolation on the data and approximating the integral as $\sum_{i=1}^{N} f(x_i)\ \Delta x$, using steps of $\Delta x = 0.0001\,\mathrm{nm}$. It was checked that the approximation of the integral converges as Δx becomes smaller (convergence is achieved at much higher values of Δx).

The molar extinction coefficient was calculated as defined in Eq. 4, using the molar density of the β-phase chain segments (see Eq. 31 for c_β):

$$c_{\beta_{molar}} \;=\; c_\beta \div N_A \;=\; 0.03321 \;\times \frac{\beta_{fraction}}{1-\beta_{fraction}} \;\times\; \mathrm{mol\,L^{-1}}. \tag{35}$$

The resulting molar extinction coefficients ϵ_a as a function of wavelength are displayed in Fig. 11.

Care needs to be taken to ensure the use of the right units in Eq. 32. I_d is a unit-less quantity, ϵ_a has units of $\frac{\mathrm{dm}^3}{\mathrm{mol\,cm}}$ if the thickness is entered in cm and the concentration in $\frac{\mathrm{mol}}{\mathrm{L}}$. The value of J was calculated again by approximating the integral as a sum, where $d\lambda$ was taken in 1 nm steps corresponding to the resolution of the absorption data.

6.2.2 Results from Time-Integrated Data

The resulting Förster radii are displayed in Table 3. There is a weakly decreasing trend for R_0 with increasing β-phase content, which is discussed in the main article.

Table 3: Förster Radii from Absorption and Emission

β-phase (%)	R_0 (nm)
7.4	5.92
10.9	6.18
12.4	5.96
14.0	6.2
18.6	5.75
22.4	5.7
24.5	5.68
25.6	5.62

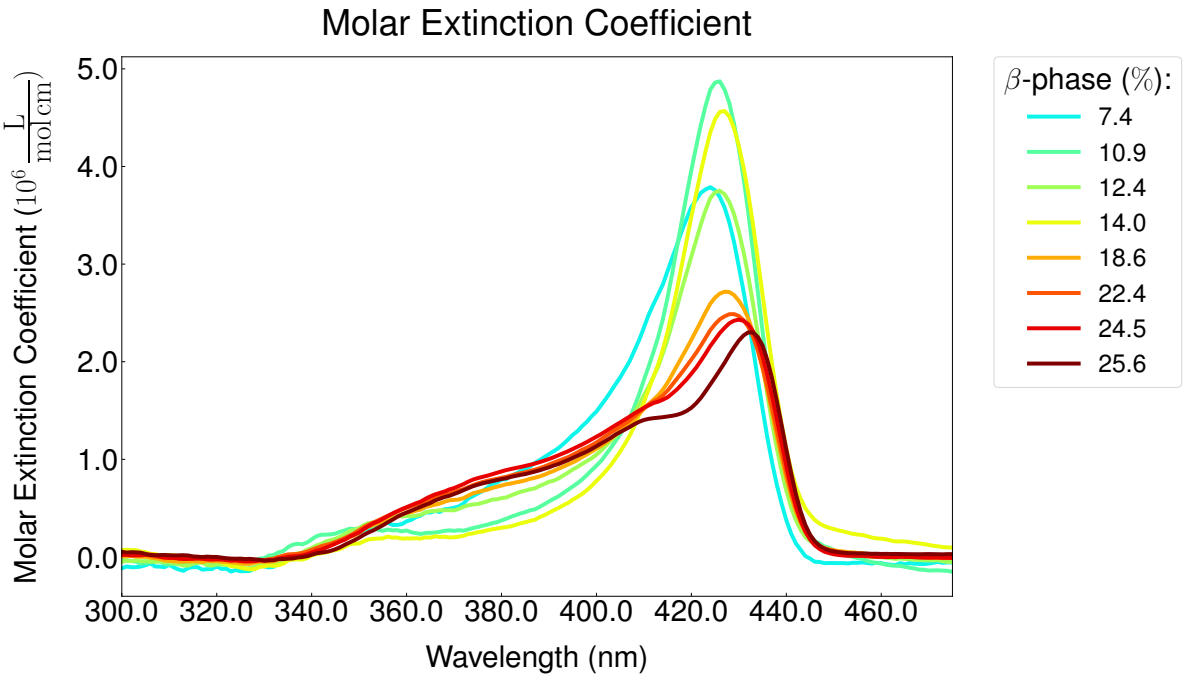

Figure 11: Molar extinction coefficient of the β-phase samples, obtained from the β-phase absorptance spectra using Eq. 4.

References

(1) https://www.cdtltd.co.uk/.

(2) Zhang, Q.; Chi, L.; Hai, G.; Fang, Y.; Li, X.; Xia, R.; Huang, W.; Gu, E. An Easy Approach to Control β-Phase Formation in PFO Films for Optimized Emission Properties. *Molecules* **2017**, *22*, 315.

(3) http://edwardsvacuum.com/.

(4) Perevedentsev, A.; Chander, N.; Kim, J.-S. S.; Bradley, D. D. C. Spectroscopic Properties of Poly(9,9-dioctylfluorene) Thin Films Possessing Varied Fractions of β-Phase Chain Segments: Enhanced Photoluminescence Efficiency via Conformation Structuring. *J. Polym. Sci. B* **2016**, *54*, 1995–2006.

(5) Huang, L.; Huang, X.; Sun, G.; Gu, C.; Lu, D.; Ma, Y. Study of β-Phase and Chains Aggregation Degrees in Poly(9,9-dioctylfluorene) (PFO) Solution. *J. Phys. Chem. C* **2012**, *116*, 7993–7999.

(6) Valeur, B.; Berberan-Santos, M. N. *Molecular Fluorescence: Principles and Applications*; Wiley-VCH Verlag GmbH & Co.KGaA: Weinheim, 2012.

(7) Bradley, D. D. C.; Grell, M.; Long, X.; Mellor, H.; Grice, A.; Road, H.; Inbasekaran, M.; Woo, E. P. Influence of Aggregation on the Optical Properties of a Polyfluorene. *Proc. SPIE* **1997**, *3145*, 254–259.

(8) Bansal, A. K.; Ruseckas, A.; Shaw, P. E.; Samuel, I. D. W. Fluorescence Quenchers in Mixed Phase Polyfluorene Films. *J. Phys. Chem. C* **2010**, *114*, 17864–17867.

(9) Köhler, A.; Bässler, H. *Electronic Processes in Organic Semiconductors*; WileyVCH Verlag GmbH: Weinheim, 2015.

(10) Ariu, M.; Sims, M.; Rahn, M.; Hill, J.; Fox, A. M.; Lidzey, D. G.; Oda, M.; Cabanillas-Gonzalez, J.; Bradley, D. D. C. Exciton Migration in β-Phase Poly(9,9-dioctylfluorene). *Phys. Rev. B* **2003**, *67*, 1–11.

(11) Gong, J. Q.; Parkinson, P.; Kondratuk, D. V.; Gil-Ramírez, G.; Anderson, H. L.; Herz, L. M. Structure-Directed Exciton Dynamics in Templated Molecular Nanorings. *J. Phys. Chem. C* **2015**, *119*, 6414–6420.

(12) Förster, T. Experimentelle und Theoretische Untersuchung des Zwischenmolekularen Übergangs von Elektroneneanregungsenergie. *Z. Naturforsch.* **1949**, *4a*, 321–327.

(13) Förster, T. 10th Spiers Memorial Lecture. Transfer Mechanisms of Electronic Excitation. *Discuss. Faraday Soc.* **1959**, *27*, 7–17.

(14) Medintz, I., Hildebrandt, N., Eds. *FRET - Förster Resonance Energy Transfer*; Wiley-VCH Verlag GmbH & Co.KGaA: Weinheim, 2014.

(15) Khan, A. L. T.; Sreearunothai, P.; Herz, L. M.; Banach, M. J.; Köhler, A. Morphology-Dependent Energy Transfer Within Polyfluorene Thin Films. *Phys. Rev. B* **2004**, *69*, 085201.

(16) Herz, L. M.; Silva, C.; Friend, R. H.; Phillips, R. T.; Setayesh, S.; Becker, S.; Marsitsky, D.; Müllen, K. Effects of Aggregation on the Excitation Transfer in Perylene-End-Capped Polyindenofluorene Studied by Time-Resolved Photoluminescence Spectroscopy. *Phys. Rev. B* **2001**, *64*, 195203.

(17) Chang, M. H.; Frampton, M. J.; Anderson, H. L.; Herz, L. M. Intermolecular Interaction Effects on the Ultrafast Depolarization of the Optical Emission from Conjugated Polymers. *Phys. Rev. Lett.* **2007**, *98*, 027402.

(18) Shah, J. Ultrafast Luminescence Spectroscopy Using Sum Frequency Generation. *IEEE J. Quantum Electron.* **1988**, *24*, 276–288.

(19) Achermann, M. *Optical Techniques for Solid-State Materials Characterization*; Taylor & Francis Group, LLC, 2012; pp 443–465.

(20) Rullière, C.; Amand, T.; Marie, X. In *Femtosecond Laser Pulses - Principles and Experiments*, 2nd ed.; Rullière, C., Ed.; 2005; pp 223–281.

(21) Förster, T. Zwischenmolekulare Energiewanderung und Fluoreszenz. *Ann. Phys.* **1948**, *2*, 55–75.

(22) Powell, R. C.; Soos, Z. G. Singlet Exciton Energy Transfer in Organic Solids. *J. Lumin.* **1975**, *11*, 1–45.

(23) Powell, R. C.; Kepler, R. G. Evidence for Long-Range Exciton-Impurity Interaction in Tetracene-Doped Anthracene Crystals. *Phys. Rev. Lett.* **1969**, *22*, 636–639.

(24) Herz, L. M. Aggregation Effects in Conjugated Polymer Films Studied by Time-Resolved Photoluminescence Spectroscopy. Ph.D. thesis, 2001.

(25) Herz, L. M.; Silva, C.; Grimsdale, A. C.; Müllen, K.; Phillips, R. T. Time-Dependent Energy Transfer Rates in a Conjugated Polymer Guest-Host System. *Phys* **2004**, *70*, 1–9.

(26) Stevens, M. A.; Silva, C.; Russell, D. M.; Friend, R. H. Exciton Dissociation Mechanisms in the Polymeric Semiconductors Poly(9,9-dioctylfluorene) and Poly(9,9-dioctylfluorene-co-benzothiadiazole). *Phys. Rev. B* **2001**, *63*, 165213.

(27) Braslavsky, S. E.; Fron, E.; Rodríguez, H. B.; Román, E. S.; Scholes, G. D.; Schweitzer, G.; Valeur, B.; Wirz, J. Pitfalls and Limitations in the Practical Use of Förster's Theory of Resonance Energy Transfer. *Photochem. Photobiol. Sci.* **2008**, *7*, 1444–1448.

(28) Maksimov, M.; Rozman, I. On Energy Transfer in Solid Solutions. *Opt. Spectrosc. USSR* **1961**, *12*, 337–338.

(29) Lunt, R. R.; Giebink, N. C.; Belak, A. A.; Benziger, J. B.; Forrest, S. R. Exciton Diffusion Lengths of Organic Semiconductor Thin Films Measured by Spectrally Resolved Photoluminescence Quenching. *J. Appl. Phys.* **2009**, *105*, 53711.

(30) Campoy-Quiles, M.; Heliotis, G.; Xia, R.; Ariu, M.; Pintani, M.; Etchegoin, P.; Bradley, D. D. Ellipsometric Characterization of the Optical Constants of Polyfluorene Gain Media. *Adv. Funct. Mater.* **2005**, *15*, 925–933.

(31) Campoy-Quiles, M.; Alonso, M. I.; Bradley, D. D.; Richter, L. J. Advanced Ellipsometric Characterization of Conjugated Polymer Films. *Adv. Funct. Mater.* **2014**, *24*, 2116–2134.

(32) Tropf, L.; Dietrich, C. P.; Herbst, S.; Kanibolotsky, A. L.; Skabara, P. J.; Würthner, F.; Samuel, I. D.; Gather, M. C.; Höfling, S. Influence of Optical Material Properties on Strong Coupling in Prganic Semiconductor Based Microcavities. *Appl. Phys. Lett.* **2017**, *110*, 153302.

(33) Macdonald, E. K.; Shaver, M. P. Intrinsic High Refractive Index Polymers. *Polym. Int.* **2015**, *64*, 6–14.

(34) Tabata, K.; Braam, D.; Kushida, S.; Tong, L.; Kuwabara, J.; Kanbara, T.; Beckel, A.; Lorke, A.; Yamamoto, Y. Self-Assembled Conjugated Polymer Spheres as Fluorescent Microresonators. *Sci. Rep.* **2014**, *4*, 5902.